NINETEENTH EUROPEAN ROTORCRAFT FORUM

Paper No. C20

3D EULER METHODS FOR MULTIBLADED ROTORS IN HOVER AND FORWARD FLIGHT

by

K. Pahlke, J. Raddatz

DLR

Institute of Design Aerodynamics

Germany

September 14-16, 1993

CERNOBBIO (Como)

ITALY

ASSOCIAZIONE INDUSTRIE AEROSPAZIALI

ASSOCIAZIONE ITALIANA DI AERONAUTICA ED ASTRONAUTICA

NINETEENTH EUROPEAN ROTORCRAFT FORUM

Paper No. C20

3D EULER METHODS FOR MULTIBLADED ROTORS IN HOVER AND FORWARD FLIGHT

K. Pahlke, J. Raddatz

List of symbols:

c	chord
c_p	pressure coefficient
C_T	thrust coefficient
E	total specific energy
$\bar{\bar{F}}$	flux tensor
$\vec{G}$	vector of source terms
H	total specific enthalpy
$\vec{n}$	unit outward to ∂V
p	pressure
$\vec{q}$	velocity vector
$\vec{q}_b$	vector of the velocity of a control volume boundary
r	radial position of a rotor section
$\vec{r}$	$= (x, y, z)^T$ coordinate vector
R	rotor radius
dS	surface element
t	time
u, v, w	Cartesian velocity components
V	control volume
dV	volume element
∂V	boundary of V
$\vec{W}$	vector of conservative variables
x, y, z	Cartesian coordinates
α_{TPP}	angle between tip path plane and onflow velocity
γ	ratio of specific heats
θ	pitching angle
μ	advance ratio
ρ	density
σ	solidity of the rotor
ψ	azimuth
ω	angular velocity ($\omega = d\psi/dt$)

1. Introduction

A full calculation of the flow around a helicopter rotor requires a three-dimensional unsteady method able to compute various flow conditions like:

- transonic flows for the advancing rotor blade,
- flows with important viscous effects for the dynamic stall problem on the retreating blade,
- influence of a very complicated wake system generated by the blades,
- several blades in relativ motion,
- blades in full aeroelastic motion.

Up to now, no single theoretical method is available for such difficult conditions. The assumption of inviscid and irrotational flow leads to prediction tools based on the full potential equation (or further simplified forms), which have been developed to a high degree of maturity. The Euler equations, although more expensive, provide the advantages of being able to treat anisotropic and rotational flow and admit vortical solutions. As it was shown in (1.) it is possible to calculate the wake of a hovering rotor with an Euler code. The methods used at the DLR Institute for Design Aerodynamics to predict the flows on helicopter blades and to study advanced blade tip shapes for high speed flight are a three-dimensional steady Euler-method for hover calculations and a time-accurate Euler-method for forward flight calculations. These algorithms offer the possibility for further developments solving the Navier-Stokes-equations or using advanced nonlinear aeroacustic approaches.

For hover cases the code development is directed towards improvement of accuracy and convergence acceleration to the steady state. Therefore, a multigrid version using a cell-vertex discretization is being implemented. For the forward fight case a time accurate code has been developed. This code uses still a cell centered formulation.

The flow around a rotor in non-lifting forward flight can be described as the flow around a moving rigid body. For calculating such a flow, the governing equations are transformed into a body fixed coordinate system. Using this approach the metric terms have to be calculated only once and the grid velocities can easily be obtained. A set of governing equations suited to this approach is described in chapter 2. For rotors in lifting forward flight it is no longer possible to use a rigid grid around the whole rotor because of the relative motion of the different blades. Therefore, in a first step a grid around only one blade is used and the downwash of the other blades is taken into account by a wake model.

Numerical aspects of the algorithms are described briefly in chapter 3. The grid generation is described in chapter 4 and the results for hover and forward flight cases are presented in chapter 5.

2. Governing equations

A general rigid body motion can be described as a translatory motion with the translatory velocity $\vec{q}_0$ and a rotation of the rigid body around 3 axis. Let (x, y, z) denote the inertial and (x_r, y_r, z_r) the moving coordinate system. The transformation from the inertial system into the moving system is given by

$$\vec{r}(t) = \vec{r}_0(t) + T(\beta, \theta, \psi)\ \vec{r}_r(t),$$

where $\vec{r}_0(t)$ denotes the origin of the moving coordinate system referred to the inertial system. $T(\beta, \theta, \psi)$ is the matrix defining the rotation with the flapping angle β, the pitch angle θ and the azimuth angle ψ. The time derivative of $\vec{r}(t)$ reads

$$\frac{d\vec{r}}{dt} = \frac{d\vec{r}_0}{dt} + \frac{d}{dt}(T(\beta, \theta, \psi))\,\vec{r}_r + T(\beta, \theta, \psi)\frac{d\vec{r}_r}{dt}$$

The relation between the velocity $\vec{q} = d\vec{r}/dt$ and the velocity $d\vec{r}_r/dt$ is geometry dependent. Such a relation is not well suited for the numerical treatment of far field boundary conditions for moving grids. Therefore, the velocity

$$\vec{q}_r = T^{-1}(\beta, \theta, \psi)\,\vec{q}$$

is introduced. The unsteady Euler equations have been transformed into the moving coordinate system (x_r, y_r, z_r). The transformed equations read

$$\frac{d}{dt}\int_{V_r} \vec{W}_r\, dV_r + \int_{\partial V_r} \vec{F}_r \cdot \vec{n}_r\, dS_r + \int_{V_r} \vec{G}_r\, dV_r = 0$$

with

$$\vec{W}_r = \begin{bmatrix} \rho \\ \rho u_r \\ \rho v_r \\ \rho w_r \\ \rho E_r \end{bmatrix}; \vec{F}_r = \begin{bmatrix} \rho(\vec{q}_r - \vec{q}_{b,r}) \\ \rho u_r(\vec{q}_r - \vec{q}_{b,r}) + p\vec{i}_{x_r} \\ \rho v_r(\vec{q}_r - \vec{q}_{b,r}) + p\vec{i}_{y_r} \\ \rho w_r(\vec{q}_r - \vec{q}_{b,r}) + p\vec{i}_{z_r} \\ \rho(H_r\vec{q}_r - E_r\vec{q}_{b,r}) \end{bmatrix}.$$

The source term $\vec{G}_r$ contains the trigonometric functions describing the rotational motion.

This system of equations is closed by

$$p = (\gamma - 1)\,\rho\left(E_r - \frac{u_r^2 + v_r^2 + w_r^2}{2}\right) \text{ and}$$

$$H_r = E_r + \frac{p}{\rho}.$$

Hover case: The flow around a hovering rotor is steady referred to the rotating coordinate system. For a hovering rotor rotating around the x-axis with the angular velocity $\vec{\omega} = (\omega, 0, 0)^T$ the vector of the velocity of the control volume boundary and the source term reduce to

$$\vec{q}_{b,r} = \begin{bmatrix} 0 \\ -\omega z_{b,r} \\ \omega y_{b,r} \end{bmatrix},\ G_r = \begin{bmatrix} 0 \\ 0 \\ -\omega\rho w_r \\ \omega\rho v_r \\ 0 \end{bmatrix}.$$

The energy equation is substituted by

$$\frac{d}{dt}\int_{V_r} \rho\tilde{E}_r\, dV_r + \int_{\partial V_r} \rho\tilde{H}_r(\vec{q}_r - \vec{q}_{b,r}) \cdot \vec{n}_r\, dS_r = 0$$

with $\tilde{E}_r = E_r - \vec{q}_r(\vec{\omega} \times \vec{r}_r)$ and

$\tilde{H}_r = \tilde{E}_r + p/\rho$.

$\tilde{H}_r$ is the so called rothalpy, which is constant in the whole flow field for the case of an adiabatic steady flow in the rotating coordinate system.

3. Numerical Aspects

3.1 Spatial and Temporal Discretization

The discretization of space and time is separated following the method of lines (Jameson et al. (2.)) using a finite volume formulation for the spatial discretization. The flow quantities $\vec{W}_r$ and the source term $\vec{G}_r$ are taken to be volume averaged, located at the center of the control volume in the cell centered code and located at the nodes of the grid in the cell-vertex formulation. The finite volume discretization reduces to a second-order central difference scheme on a Cartesian grid with constant grid sizes. If an arbitrary nonuniform grid is used, the accuracy of these schemes depends on the smoothness of the grid. For the cell-vertex scheme first order accuracy is guaranteed for arbitrary grids (for details see (3.)). In order to avoid spurious oscillations a blend of first and third order dissipative terms is introduced. An explicit Runge-Kutta time stepping scheme is used with an evaluation of the dissipatve fluxes at the first two stages (4.).

3.2 Boundary Conditions

Three types of boundary conditions occur in the codes. These are the condition on solid body, the condition across a coordinate cut and the inflow/outflow conditions in the far field.

The no-normal flow condition is imposed on a solid body. This condition reduces to a zero flux condition on a body-fitted grid. Consequently only the pressure terms remain in the momentum flux balances. For the cell centered formulation the pressure at the body surface is estimated using a first order extrapolation.

The far field boundary is treated following the concept of Characteritic Variables for non-reflecting boundary conditions. The free stream values are

$\vec{q}_{r,\infty} = T^{-1}(\beta, \theta, \psi)\,\vec{q}_{\infty}$, $E_{r,\infty} = E_r$ and

$H_{r,\infty} = H_r$.

By the choice of $\vec{q}_r$ the absolute values of $\vec{q}_r$ and $\vec{q}$ are the same and $\vec{q}_r$can be calculated by $\vec{q}$, β, θ and ψ, independently of x, y and z.

3.3 Wake Modelling

In Euler-computations on grids containing the whole rotor disc the wake is part of the solution. Consequently no wake model is used for hover cases. Up to now the code is not able to handle several blades in relative motion, which is necessary for the lifting forward flight case. Therefore the flow around only one blade is calculated using a wake model providing the downwash and the wake effects of the whole rotor. Two wake models are used. The first is the METAR code (fixed wake) which models the effect of the wake by an effective angle of attack (5.). Such a distribution of an effictive angle of attack for one test case has kindly been made available by ONERA. The downwash is taken into account by prescribing a constant angle of attack for the whole blade such that the angle of attack at $0.9R$ meets exactly the value given by METAR. The second is based on Beddoes wake model (fixed wake) (6.),(7.) and provides a field of induced velocities $\vec{q}_{r,\,induced}$ normal to the tip path plane which are used to change the solid body boundary condition in the Euler code:

$$(\vec{q}_r - \vec{q}_{b,r})\,\vec{n} = \vec{q}_{r,\,induced}\,\vec{n}.$$

The induced velocities have been provided at every $5°$ azimuth. For angles in between the induced velocities are interpolated using either linear interpolation in ψ (non-BVI case) or an interpolation where the location of the interaction in radial direction is computed first and then a linear interpolation in ψ and r is used (BVI case).

3.4 Acceleration Techniques

In order to accelerate the convergence to steady state for hover cases rothalpy damping, implicit residual averaging (8.) and a multigrid algorithm have been implemented. The technique of implicit residual averaging has been adapted to time-accurate calculations for forward flight cases (9.), (10.).

4. Grid Generation

Body conforming, single block, computational grids were constructed for multibladed hovering rotors, using a grid generator based on an elliptic 3D solver (for details see (11.)). Because of the cylindrical nature of the flow of a hovering rotor an O-H topology was chosen with the wraparound O in chordwise direction and the H-type in spanwise direction.

Due to the symmetry of the flow only a segment of the rotor plane containing one blade has to be regarded. The other blades are taken into account by periodicity conditions in the blade azimuthal direction, which swaps the flow information at the front and back boundaries of the cylindrical mesh. On account of this grid topology it is obvious to generate grids with identical point distributions on

the periodicity planes. Therefore, no interpolation of the flow quantities on the periodicity planes is required.

Figure 1 presents the shape of the grids in the rotor pane for a 2-bladed rotor on the left side and a 3-bladed rotor on the right side. The whole grid for the 3-bladed rotor is shown in Figure 2, representing the surface grid of the rotor blade and the most part of the outer surface. The construction of grids for blades with advanced tip shapes is possible and demonstrated for the ONERA PF1 rotor blade (Figure 3). The standard grids used for hover calculation had 129 points in the wraparound (along the chord) direction, 57 points in the spanwise (radial) direction (33 points on the blade surface), and 41 points in the normal direction. The grid is clustered near the leading and trailing edges and near the tip region to resolve the tip vortex. A coarse grid with 65 x 29 x 21 points was constructed from the fine grid by removing every other point in all three directions. In the same way the coarser grid levels for the multigrid option used for hover calculations are produced.

Grids used for forward flight calculations are constructed quite similar but with a far field of cylindrical shape. The blades were continued to the hub with an axisymmetric section at $r = 0$. This allows to generate a one-block grid for a 2-bladed rotor.

5. Results

The following test cases have all been calculated on a single processor of a CRAY Y-MP.

5.1 Hover

The hover test cases correspond to the experimental hover conditions conducted by ONERA on a 3-bladed model rotor, on the one hand with a rectangular tip and on the other hand with an anhedral sweptback tip shape called PF1 tip. Both blades are made of SA131XX airfoil sections with an aspect ratio of 6.97 . They are twisted but have no taper. The experimental conditions for the rectangular blade were: tip Mach number $M_{\omega R} = 0.610$, collective pitch $\theta_c = 10.37°$, the conditions used for the PF1 blade were: $M_{\omega R} = 0.614$, $\theta_c = 11.68°$.

Surface pressures are shown in Figure 4 and 5 for the two experimental conditions considered. The calculations were done on a fine grid consisting of 301473 points and on a coarser grid of nearly 40000 points which was generated from the fine grid. The theoretical data for the fine grids and the experimental data agree well on all radial stations. A general deteriotion of the predicted surface pressures can be seen for the coarse grids. Particular the suctions peaks at the leading edge near the tip are much lower as those for the fine grids. The comparison indicates that a still finer grid is necessary to achieve a fully grid converged solution. However, typical time converged, singlegrid solutions on the coarser grids take about 20 minutes of CPU time, down from 3 h for the fine-grid cases, caused by a large number of time steps (up to 3000) to reach convergence

To reduce this very high computing times for hover calculations several modifications of the existing code were made in the last months, essentially :

- change of the discretisation from a cell centered to a cell vertex scheme to improve the results of corse-grid calculations.
- implementation of a multigrid technique, especially to reduce the number of time steps for calculations on fine grids.

Figure 6 and 7 show the results of the first calculations made with the improved Euler code. For the comparison between both codes the same grids and the same test conditions of the ONERA 3-bladed model rotors were used. It is visible that the calculations on the fine grid with the cell centered and with the cell vertex scheme agree very well for section r/R = 0.95. Further inboard a slightly poorer agreement can be recognized. In the present stage of code validation no final explanation of this behaviour can be given. An obvious reason is the different density of grid points in the radial direction due to the grid clustering near the tip region. This becomes clear comparing the calculations made with the cell vertex scheme one the fine and the coarse grids. The differences in the pressure distributions are very small, indicating that the new cell vertex code needs less grid points for accurate hover calculations.

Considerable improvements were obtained concerning the computing times. Using a four stage multigrid method for calculations on the fine grid the number of time steps could be reduced from about 3000 to less than 300. The computing time decreases to 40 - 50 minutes for this conditions, which is about four times faster than the singlegrid calculations. The convergence history for both methods is presented in Figure 8. On the coarse grids, where a three stage multigrid method was used, a factor of three can be obtained in the reduction of computing time. The results of the multigrid cell vertex code, presented in figure 3 and 4, show a good agreement between fine and coarse grid

calculations. If the coarse grid results can be accepted for engineering purposes, a 3D-Euler calculation of the flow field of an hovering rotor takes about 5 - 7 minutes computing time using the developed cell vertex code with multigrid time-stepping scheme.

5.2 Forward Flight

In this section time-accurate results of rotors in forward flight are presented. The criterion for time convergence was the pressure coefficient at a radial station of 90 % radius. The code was run with Courant numbers CFL and CFL/2. The instantanious pressure distributions for $\psi = 30°, 60°, ..., 360°$ were compared. If the differences in c_p were below 0.5 % referred to $|c_p|_{max}$, the result was accepted to be time converged. If not the calculation was repeated with CFL/4....

Non-Lifting Forward Flight

Two non-lifting forward flight test cases have been calculated. The first case is a rotor with two untwisted rectangular blades with an aspect ratio of seven. The blades have a constant airfoil (NACA 0012) (12.). The second rotor is the two-bladed ONERA test rotor. This rotor has untwisted rectangular blades with NACA 00XX airfoils (for details see (13.).

The motion of a rotor in forward flight is prescribed by defining the whole movement via the governing equations. Using this approach, a fully periodic state is reached after 1 1/2 periods. This very short transient phase is due to the fact that no wake has to be captured.

The effect of grid refinement was studied starting with a grid consisting of 64x16x30 cells for one blade of the NACA 0012 rotor. The grid was refined in each index direction separately. As the differences between calculations with a grid around the whole rotor and with a grid around only one rotor blade are very small for the non-lifting case, this grid refinement investigation was done with a grid around one rotor blade only. In the radial direction the number of grid points was not doubled on the whole blade but the points were rearranged and clustered at 0.9 R. The grid fineness in radial direction between 0.8 R and R was exactly doubled. The strongest effect of the grid refinement was observed for the radial refinement indicating the strong three dimensionality of this non-lifting flow. Figure 9 shows a comparison of the pressure-distribution for the coarse grid, the fully refined grid and the experimental data from (12.). The results obtained with the fine grid are in good agreement with the experimental data.

For the two bladed ONERA test rotor a grid was generated which was relatively coarse in the root region and strongly refined at $0.9R$ (64x16x27 cells for the half grid around one blade). A comparison of the 3D computation and the experimental data is shown in Figure 10. The results of the 3D computation are in acceptable agreement with the experimental data. The results obviously could still be improved by refining the grid. 3080 CPU-seconds were needed for one period with the 64x16x54 cells grid (CFL=50).

Lifting Forward Flight

The first lifting forward flight test case chosen, is the flow around the 3-bladed ONERA test rotor. It is a rotor with relatively stiff twisted rectangular blades with SA131XX airfoils. The blade definition can be found in (14.). The conditions for this test case are $M_{\omega R} = 0.63$, $\mu = 0.43$ and $C_T/\sigma = 0.065$. The rotor was controlled with a collective pitch but without a cyclic pitch. This produces a strong flapping motion of the blades. The flow conditions were defined using the rotational motion and the advance ratio of the experiment. The downwash of the rotor is accounted for by a wake model.

The transient phase for this 3D calculation was again below two rotor revolutions due to the fact that the wake is not captured. The comparison of the pressure distributions for the 3D computations and the experiment at three azimuthal positions at 90 % radius is presented in Figure 11. The agreement between the 3D calculations and the experimental data (15.) is fairly good. The strong suction peak for $\psi = 60°$ and $90°$ on the lower surface measured in the experiment is not reproduced in the computations. The comparison of the results using the METAR and the Beddoes wake model show differences which imply that the downwash predicted with the Beddoes model is stronger than with METAR. For $\psi = 150°$ the METAR results agree better with the experiment. About 1900 CPU-seconds were needed for one period with the 64x16x33 cells grid (CFL=50).

The following two cases for the AH1OLS model rotor have been calculated using the Beddoes wake model. Figure 12 a) - d) show results for a moderate high speed level flight with the flow conditions $\mu = 0.298$, $M_{\omega R} = 0.664$ and $\alpha_{TPP} = -5°$. A comparison of the experiment

and the computation is shown for four transducers. Figure 12 d) shows additionally the values of the induced velocities. The computational results agree qualitatively well with the experiment, although there are clear quantitative differences.

Results for a descent flight with blade vortex interaction (BVI) are shown in Figure 13 a) - f) for the flow conditions $\mu = 0.162$, $M_{\omega R} = 0.663$ and $\alpha_{TPP} = 1°$. Figure 13 a) shows the comparison of computational results for a medium and a fine grid with experimental data. The effect of the grid refinement is very small due to the fact the the wake is prescribed. The effect of the time step size is investigated in Figure 13 b) . A computation with CFL=25 reproduced exactly the results of CFL=50. This means that a time resolution of about 4000 steps per period (CFL=50) is necessary to resolve the BVI effects. The effect of different interpolation routines (see chapter 3.3) is shown in Figure 13 c). Significant differences occur in the BVI regions when calculations with induced velocities provided for every $5°$ and every $10°$ azimuth are compared Figure 13 d). The computational results (Figures a), d), e) and f)) behave qualitatively like the experiment but there are significant differences in the absolut values of $c_p \cdot M^2$. The changes in pressure during the BVI are computed neither with exactly the same time behaviour nor amplitude as the experiment. Values of the induced velocities are plotted in Figure 13 f). These investigations show that the accuracy of the results for this test case is determined by the wake model.

6. Conclusion

The flowfield of a hovering rotor is calculated solving the Euler equations formulated in terms of the absolute flow variables in a blade attached coordinate system. Results for two hover cases with multibladed rotors have been presented, which show a good agreement between calculation and experiment. Due to the implementaion of a multigrid technique the computing times for hover calculations could be reduced considerably. The change of the discretisation scheme from a cell centered to a cell vertex scheme shows advantages in the acuracy of the results, if the same computational grids were used. On the other hand a further convergence acceleration can be obtained, because coarser grids can be used without losses of accuracy.

A time-accurate 3D Euler method for rotors in forward flight has been developed. Results for two non-lifting and three lifting forward flight cases have been presented. The agreement between computation and experiment is good for the non-lifting cases. Two fixed wake models have been compared for one lifting forward flight case showing qualitatively the same behaviour but quantitative differences. The agreement of the results using the Beddoes wake model for non-BVI cases is fairly good. For the BVI case the results show significant differences compared with experimental data. It was shown that the accuracy of the computational results is dominated by the wake model. In order to improve the accuracy the wake model has to be improved or full Euler simulations without wake modelling have to be carried out.

Acknowledgement:

The authors thank Berend van der Wall (DLR, Institue of Flight Mechanics), for providing the induced velocities of the Beddoes wake model.

7. Bibliography

1. Kroll, N. *Computation of the Flow Fields of Propellers and Hovering Rotors using Euler Equations.* 12th European Rotorcraft Forum, paper 28, 1986.

2. Jameson, A.; Schmidt, W.; Turkel, E. *Numerical Solutions of the Euler Equations by Finite Volume Methods Using Runge-Kutta Time Stepping Schemes.* AIAA-Paper 81-1259 (1981).

3. Rossow, C.-C. *Berechnung von Strömungsfeldern durch die Lösung der Euler-Gleichungen mit einer erweiterten Finite- Volumen Diskretisierungsmethode.*DLR-FB 89-38, Braunschweig,1989.

4. Kroll, N.; Jain, R. K. *Solution of Two-Dimensional Euler Equations - Experience with a Finite Volume Code.* DFVLR-FB 87-41, Braunschweig, 1987.

5. Bousman, W.G.; Young, C.; Gilbert, N.; Toulmay, F.; Johnson, W.; Riley, M.J. *Correlation of Puma Airloads-Lifting Line and Wake Calculations.* 15th European Rotorcraft Forum, Sept. 12-15, 1989, Amsterdam, The Netherlands.

6. Beddoes, T.S. *A Wake Model for High Resolution Airloads.* International Conference on Rotorcraft Basic Research,Research-Triangle-Parc, N.C. 1985

7. Van der Wall, B. *Analytische Formulierung der instationären Profilbeiwerte und deren Anwendung in der Rotorsimulation.* DLR-FB 90-28.

8. Kroll, N. *Berechnung von Strömungsfeldern um Propeller und Rotoren im Schwebeflug durch die Lösung der Euler-Gleichungen.* DLR-FB 89-37.

9. Jorgenson, P.C.E.; Chima, R.V. *An Unconditionally Stable Runge-Kutta Method for Unsteady Flows.* AIAA-89-0205, 27th Aerospace Sciences Meeting, Reno, Nevada, Jan. 9-12, 1989.

10. Pahlke, K.; Blazek, J.; Kirchner, A. *Time-Accurate Euler Computations for Rotor Flows.* 1993 European Forum : Recent Developments and Applications in Aeronautical CFD, Bristol, UK, 1-3 September 1993.

11. Findling, A.; Herrmann, U. *Development of an efficient and robust solver for elliptic grid generation.* Proceedings of the Third International Conference on Numerical Grid Generation in Computational Fluid Dynamics and Related Fields, Barcelona, Spain, 1991.

12. Caradonna, F. X.; Laub, G.H.; Tung, C. *An Experimental Investigation of the Parallel Blade-Vortex Interaction.* NASA TM-86005, Nov. 1984.

13. Caradonna, F.X.; Philippe, J.J. *The Flow over a Helicopter Blade Tip in the Transonic Regime.* Second European Rotorcraft and Powered Lift Aircraft Forum, Paper No. 21, September 20-22, Bückeburg, 1976.

14. Costes, M.; Houwink, R.; Kokkalis, A.; Pahlke, K.; Sapporiti, A. *Application of European CFD Methods for Helicopter Rotors in Forward Flight.* Eighteenth European Rotorcraft Forum, Paper 50, Avignon, 15.-18. September, 1992.

15. Philippe, J. J.; Chattot, J. J. *Experimental and Theoretical Studies on Helicopter Blade Tips at ONERA.* Sixth European Rotorcraft and Powered Lift Aircraft Forum, Paper No. 46, September 20-22, Bristol, 1980.

8. Figures

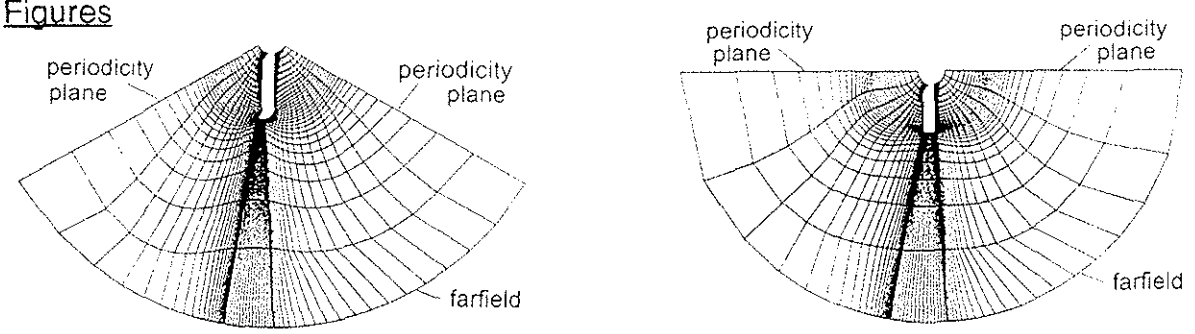

Figure 1 : Grids in the rotor planes of a 2-bladed and a 3-bladed rotor

Figure 2 : O-H grid around one blade of the 3-bladed ONERA rotor with PF1 tip

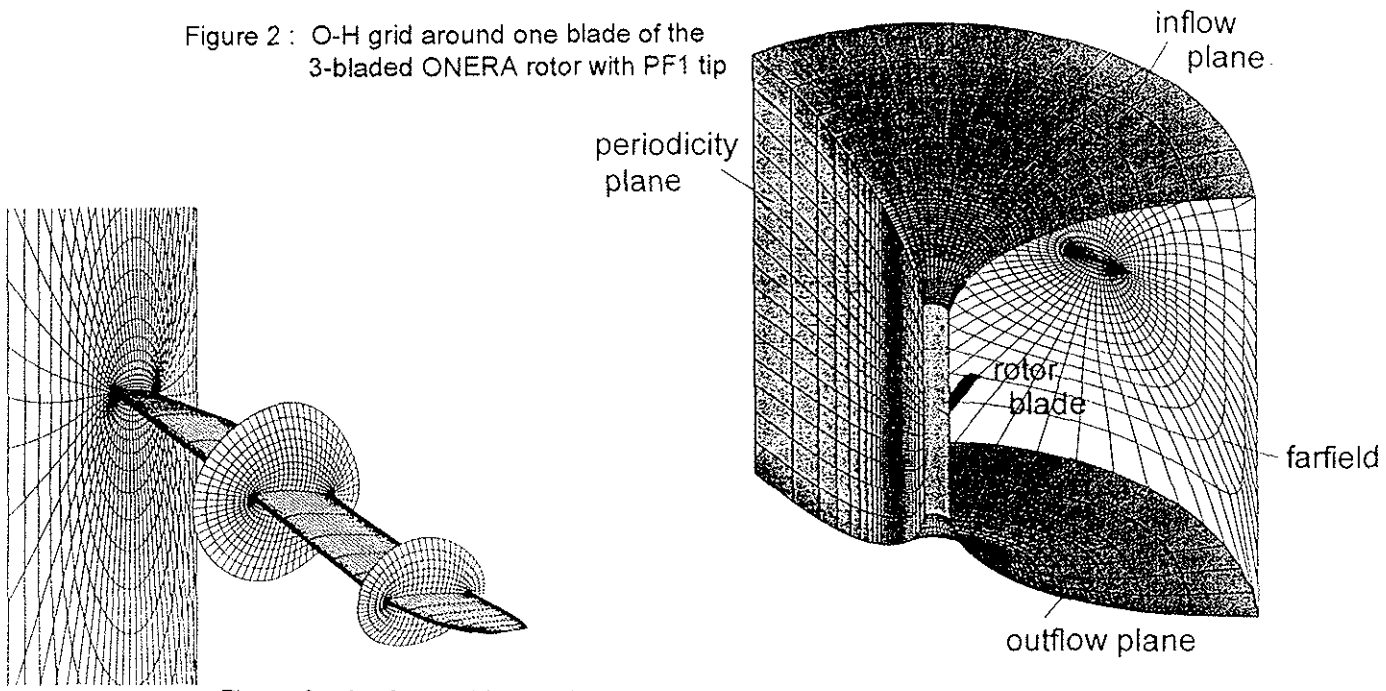

Figure 3 : Surface grid of PF1 rotor blade

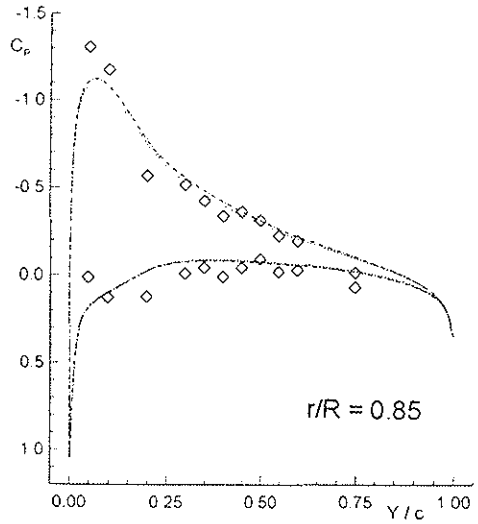

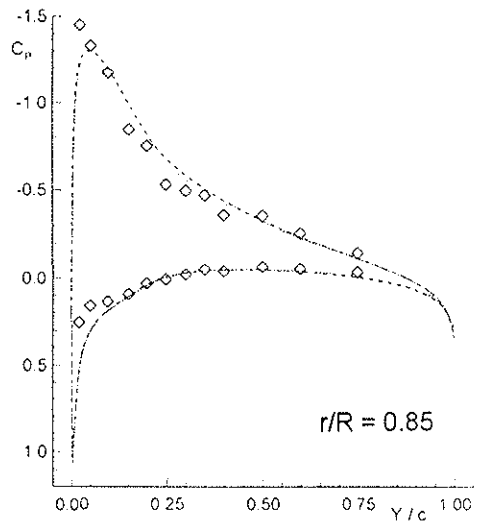

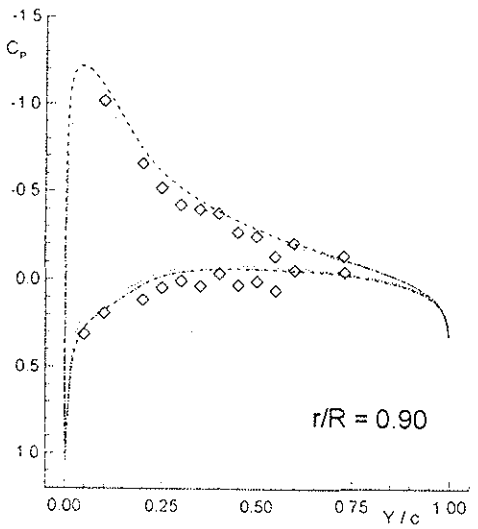

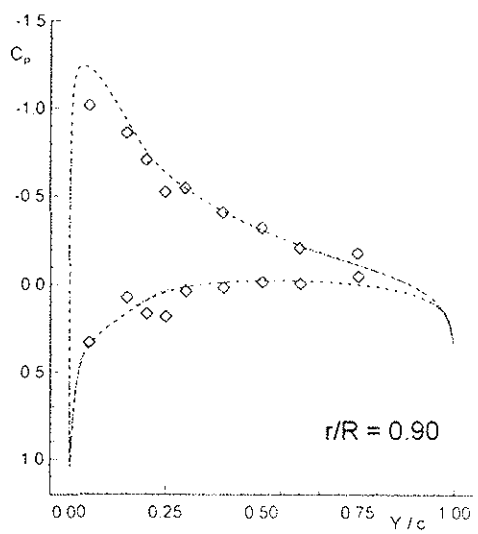

cell centered scheme (grid 129x41x57 points)

cell centered scheme (grid 65x21x29 points)

◇ measurement

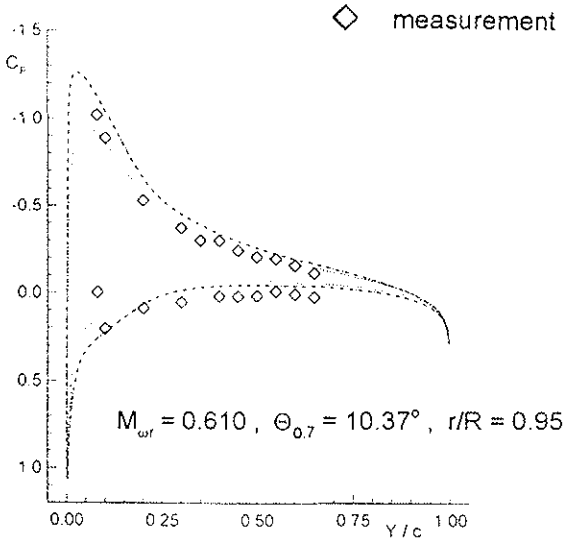

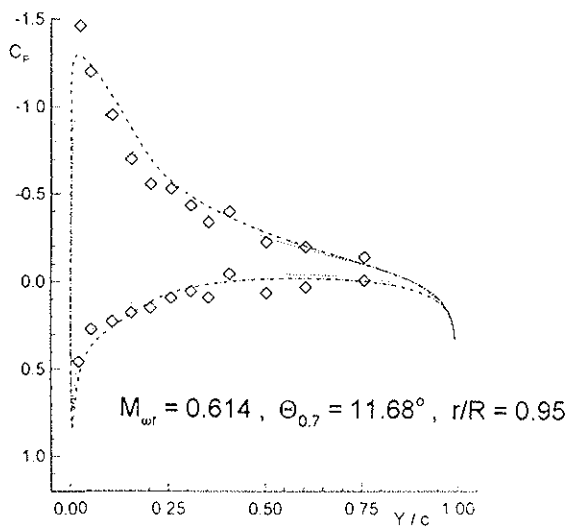

Figure 4 : Pressure distributions of 3-bladed ONERA rotor with rectangular planform shape in hover

Figure 5 : Pressure distributions of 3-bladed ONERA rotor with PF1 tip in hover

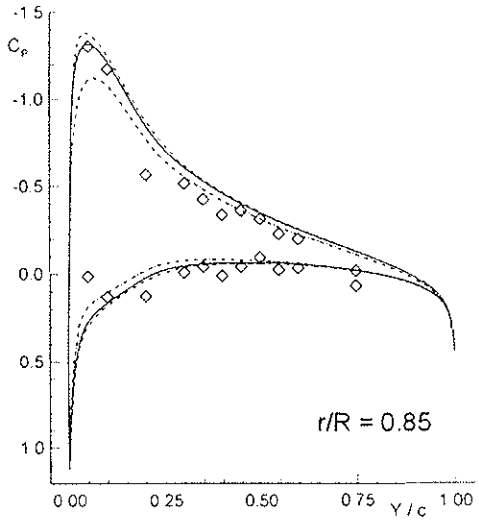

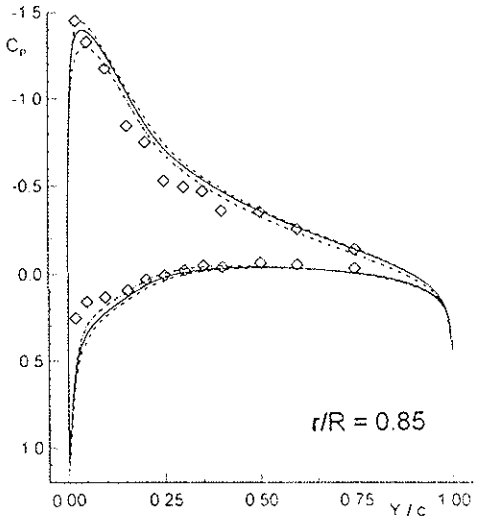

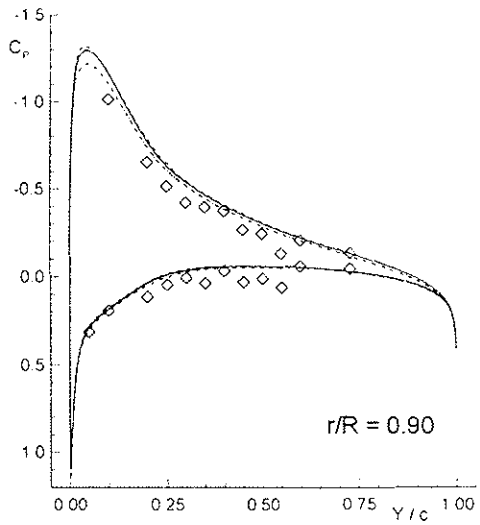

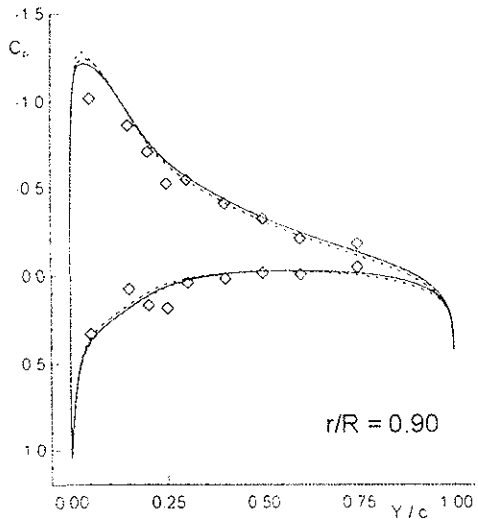

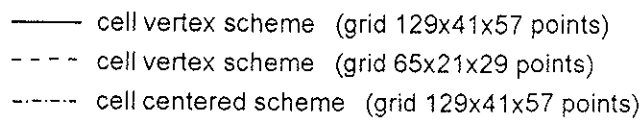

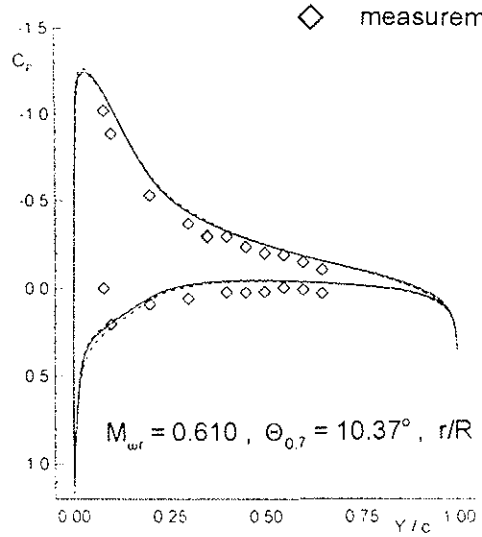

Figure 6 : Pressure distributions of 3-bladed ONERA rotor with rectangular planform shape in hover

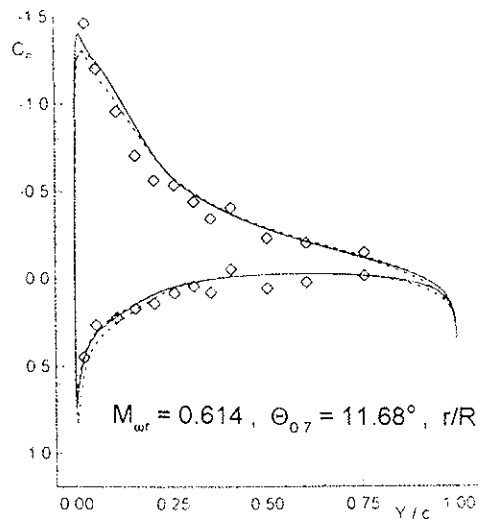

Figure 7 : Pressure distributions of 3-bladed ONERA rotor with PF1 tip in hover

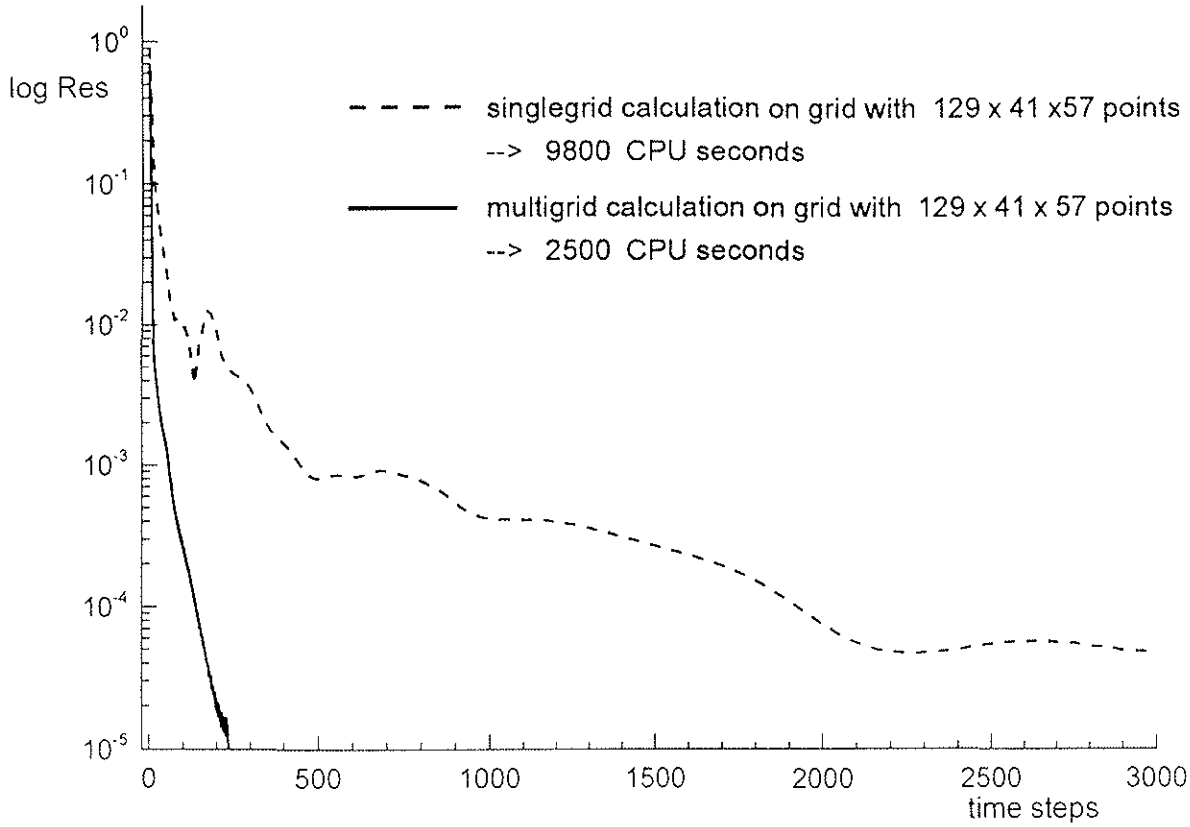

Figure 8 : Convergence history of an hover calculation

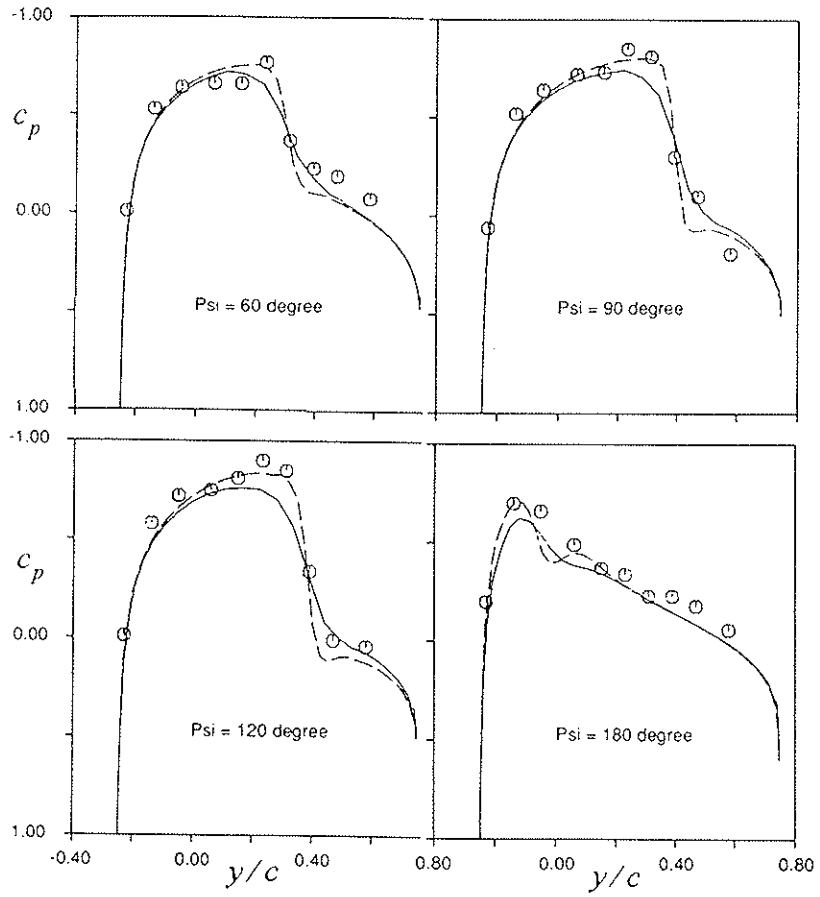

3D Euler code
(O-H grid 65x17x32 points)

3D Euler code
(O-H grid 129x33x38 points)

o Experiment

Two-bladed Rotor in Non-Lifting Forward Flight, Untwisted Rectangular Blades with NACA 0012 Airfoils

$M_{\omega R} = 0.8, \mu = 0.2,$

$R/c = 7.0, r/R = 0.9$

Figure 9

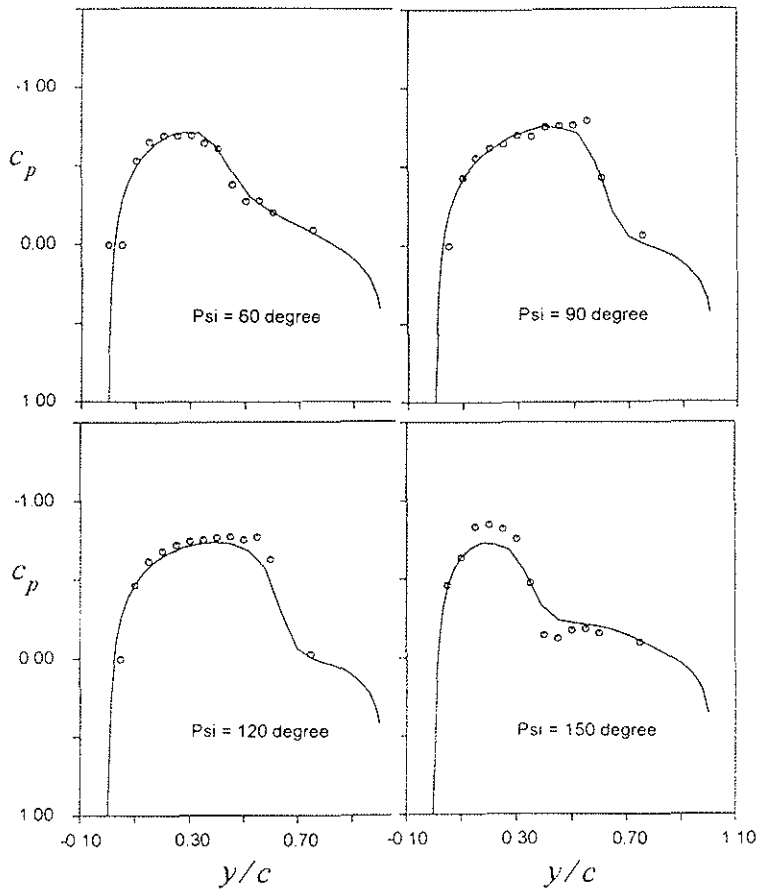

——— 3D Euler code

(O-H grid 65x17x55 points)

o Experiment

ONERA Model Rotor in Non-Lifting Forward Flight, Two Untwisted Blades with NACA 00XX Airfoils,
$M_{\omega R} = 0.625$, $\mu = 0.5$,
$r/R = 0.9$

Figure 10

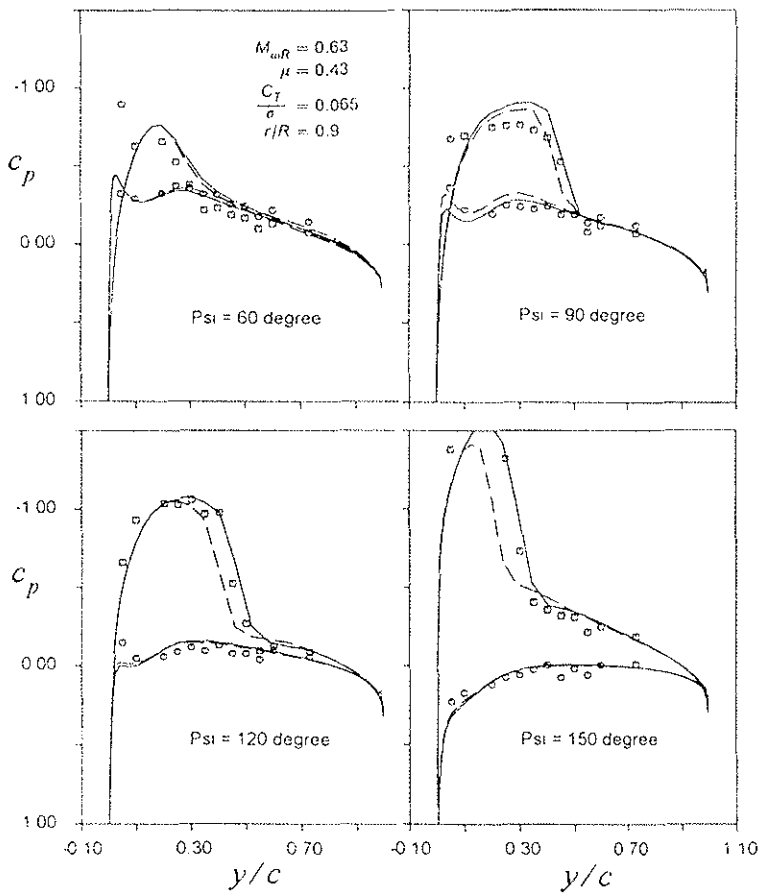

——— 3D Euler code

(O-H grid 65x17x28 points)
with METAR

- - - - - 3D Euler code
(O-H grid 65x17x28 points)
with Beddoes Wake Model

□ , o Experiment
(upper, lower side)

Three-bladed ONERA Model Rotor in Lifting Forward Flight, Twisted Rectangular Blades with SA131XX Airfoils,

Figure 11

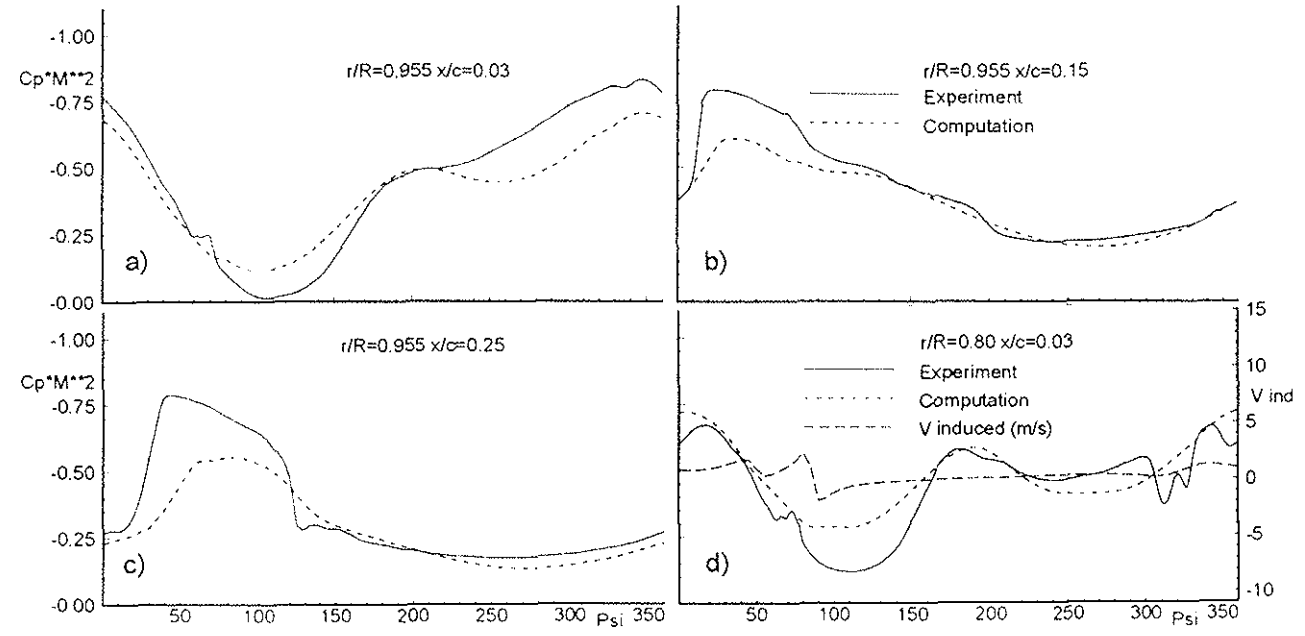

Figure 12: Two-bladed AH1OLS Model Rotor in Lifting Forward Flight

$M_{\omega R} = 0.664$, $\mu = 0.298$, $\alpha_{TPP} = -5°$

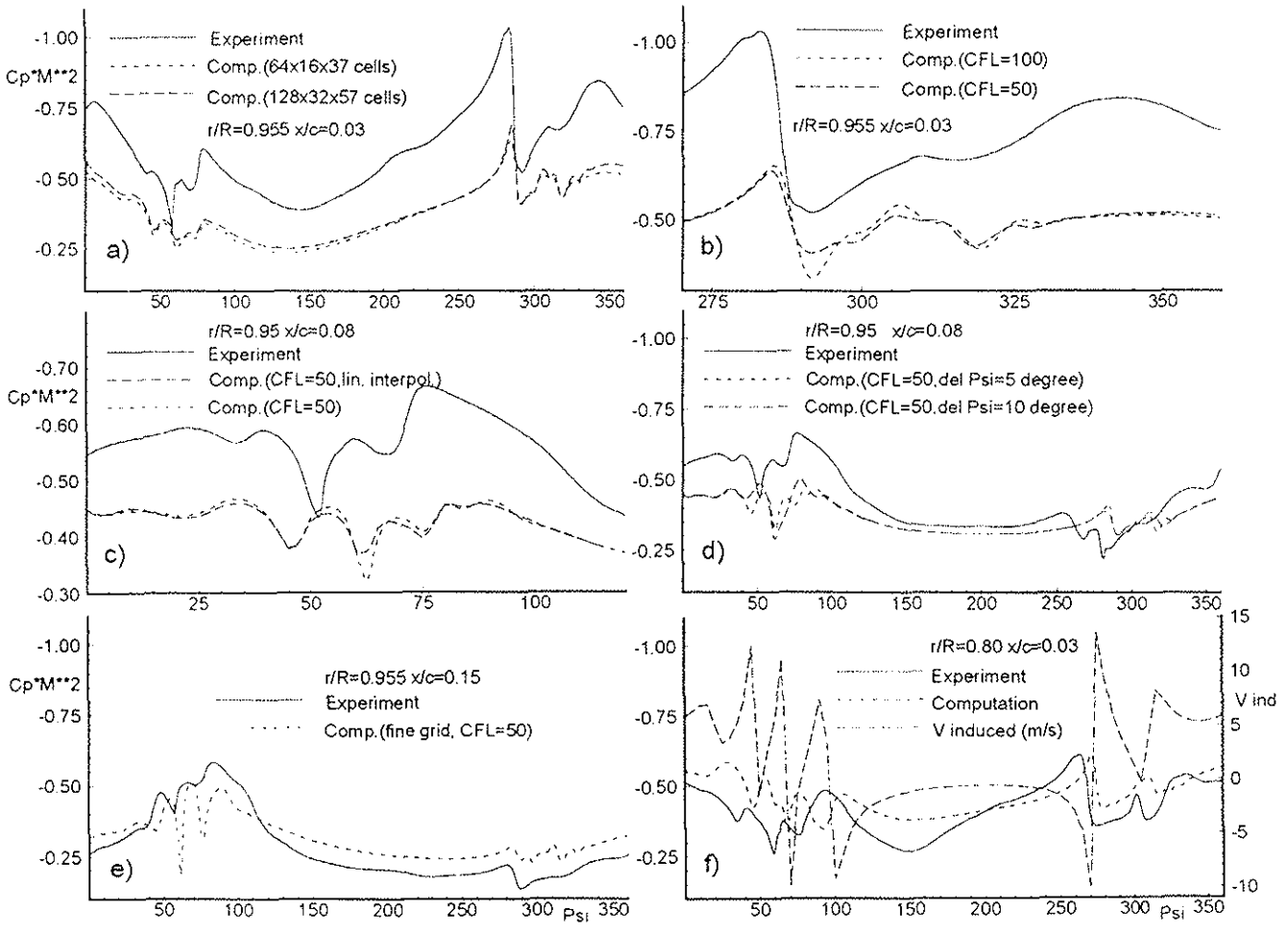

Figure 13: Two-bladed AH1OLS Model Rotor in Lifting Forward Flight

$M_{\omega R} = 0.663$, $\mu = 0.162$, $\alpha_{TPP} = 1°$